

# CAVITATION PREVENTATION IN CENTRIFUGAL PUMPS USING ANSYS

**Aldair Doría Barrios<sup>1\*</sup>, Andrés Rodríguez Toscano<sup>1</sup>, Rafael Ramírez Restrepo<sup>2</sup>**

<sup>1</sup> Universidad de la Costa - Departament of Energy, CL 58 #55-66, 080002 Barranquilla, Colombia

<sup>2</sup> Universidad del Atlántico - Department of Mechanical Engineering, Cra 30 # 8-49, 081007 Puerto Colombia, Colombia

\* adoria@cuc.edu.co

*In this paper, a computational fluid dynamic (CFD) model was developed to assess cavitation phenomenon and its local effects on a centrifugal pump. The model included the temperature of the fluid, rotational velocity, and geometric configuration of the suction. The model was validated using the pump characteristics curves of the manufacturer with an error of 5%. Also, the minimum pressure contours and the vapor volume fraction were plotted. These contours show the pump boundary conditions (temperature and angular velocity) before cavitation occurs. Thus, the impeller zone where the cavitation phenomenon is more susceptible to occurrence was identified. In addition, this analysis determined characteristic parameters such as the limit on fluid temperature, the limiting angular velocity of the pump and the ratio between the diameters of the suction pipe and the pump inlet diameter. The proposed methodology is aimed as a reference for the study of local operating parameters to avoid cavitation in various types of hydraulic pumps.*

**Keywords:** cavitation, centrifugal pump, NPSH, CFD Modelling, ANSYS

## 1 INTRODUCTION

Centrifugal pumps are widely used in the industry due to their versatility, stability, and maintenance [1]; therefore, it is crucial to prevent cavitation that can diminish the pump's performance, stability, efficiency, and lifespan. Since then, cavitation has become paramount for designers, researchers, and manufacturers of hydraulic equipment. Cavitation is the change in phase from liquid to vapor caused by accelerating liquids to high speeds and generating vapor bubbles in low-pressure regions. These bubbles travel to high-pressure regions where they suddenly collapse generating pressure waves traveling faster than the speed of sound. This phenomenon occurs under different conditions, but its consequences follow a common pattern: noise, reduction in efficiency, vibration, and extensive erosion of the rotatory blades [2].

To prevent detrimental effects on the pump's performance and damage to the impeller, the amount of vapor should be reduced [3]. The formation of vapor bubbles, however, causes only a faint noise that cannot be used to distinctly detect cavitation in field applications, as the phenomenon is only noticeable when there is a detriment in pump performance, which is an advanced cavitation stage [4]. A practical rule, used in the industry, is to consider cavitation to have begun when the pump head reduces by 3% with respect to the optimal capacity. Even so, bubbles can appear earlier, causing severe damage to the pump.

As a result of the complexity of the interaction between the fluid and the equipment, predicting the conditions which generates cavitation is a challenge. Additionally, the numerical calculations for nominal operations have many uncertainties that reduce the validity of the method. Therefore, the manufacturer should offer performance margins with minimal risk, for this reason, only approximate calculation methods that are supported by empirical data can be suggested [5].

There are several empiric and methodical attempts, such as vibration analysis, to correlate the intensity of the noise with the resulting damage [6] – [9]. A clear sign of the occurrence of cavitation is the NPSH for the installation setting and the requirement of the pump. Since improvements in the arrangement of the components can be established to ensure proper performance under the defined conditions [10].

CFD analysis of the flow in centrifugal pumps has used several simulation programs to build different physical and numerical models [11]. Several physical and numerical models have been achieved to investigate flows in cavitation and, those with two phases with state transition of these [12]. There are two types of models, one using inter-phase adjustment and the other using continuous modeling. The inter-phase methods assume a clear separation between the liquid and gas that can be found by iterative techniques. On the other hand, the continuous modeling methods define a bi-phase flow with a variable average density between two limits. These limits are implemented through homogeneous models, such as the two fluids and the hybrid method. Therefore, the continuous method is the technique used in this paper to develop the numerical CFD simulation [13].

Several pieces of research about the cavitation phenomenon are found in the scientific literature, which focus on different topics, such as the dynamics of the bubble [14][15], describing the performance of the pump during the cavitation [16][17], and its sound and erosion impacts [18] – [21]. All these references are based on conclusions when the phenomenon has occurred and not addressed the strategies to prevent it. Therefore, the objective of this

research is to use CFD tools to generate strategies to prevent the cavitation phenomenon in centrifugal pumps by varying operating parameters such as system arrangement, suction fittings, flow temperature and pump speed.

## 2 METHODS AND MATERIALS

This section specifies the requirements and constraints for the pump, the selection of the pump and its technical characteristics, the identification of the relevant study parameters, the geometric characterization and CAD modeling, the CFD modeling and its component parameters, the model validation, and the proposed variations for the CFD simulations. Also, this section presents the validation and variation of these models. Figure 1 shows the method used during the development of this research.

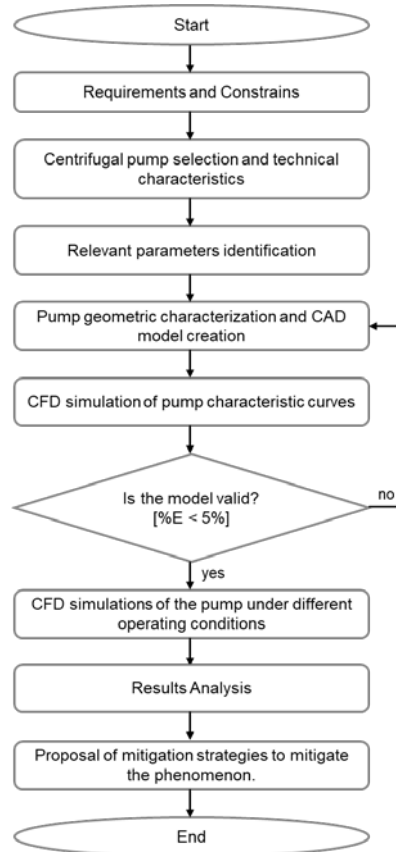


Fig. 1. Research method

To conduct the validation process, the configuration shown in Figure 2 was considered. Figure 2 shows the assembly of a single pump, identifying the area marked in blue as the water inlet (suction) and the red area as the outlet (discharge). This model is also used to analyze the system under temperature and rotational speed variations.

Furthermore, variations in the geometrical configuration of the system's suction geometry were based on the configuration considering the pump, suction pipe, and reducer (concentric or eccentric). Figure 3 shows the assembly including the suction pipe and the location of the accessory, with the water inlet on the pipe side and the outlet coinciding with the pump discharge.

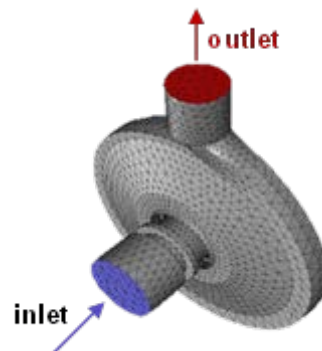


Fig. 2. CFD modeling of the assembly with the pump

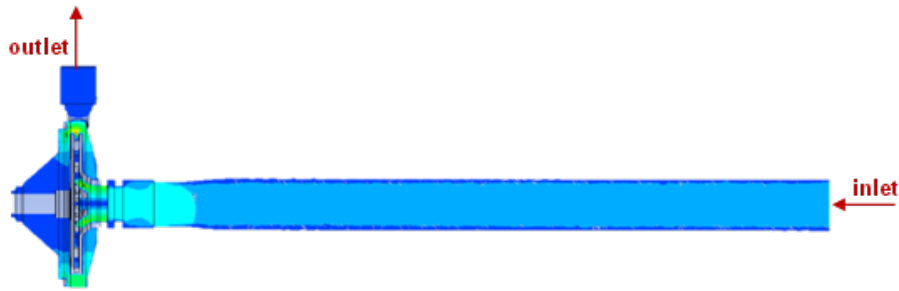


Fig. 3. CFD modeling of the assembly with the pump

### 2.1 Restrictions and requirements

For the analysis it is required to evaluate a hydraulic pump that can deliver a minimum flow rate of 70 L/min, at a minimum head of 7.5 m and a power not greater than 1 hp. This type of pumps is required for commercial applications such as irrigation, firefighting systems, water recirculation systems, sanitary installations, among others [22].

### 2.2 Pump selection and technical features

The centrifugal pump model 1A0077 from Barnes® is selected. This choice is justified because it meets the flow requirements. The technical characteristics of the pump are: Maximum head 22 m, maximum flow 35 GPM rotating at a nominal speed of 3,500 rpm.

### 2.3 CAD Modeling

Each of the constituent elements of the pump was disassembled and measured. With this, the CAD model was generated in SOLIDWORKS®. Figure 4 shows the modeled impeller considering the measurements taken.



Fig. 4. Impeller developed on the CAD model

### 2.4 Modeling and meshing

The CAD model is exported to ANSYS grid generator, where a discretized mesh was obtained. A tetrahedral mesh was used since this kind of meshing requires a lower computational cost and is very suitable for flow analysis. It was checked that the domain is free of defects, i.e., that the volume is closed. The pump mesh is shown in Figure 5.

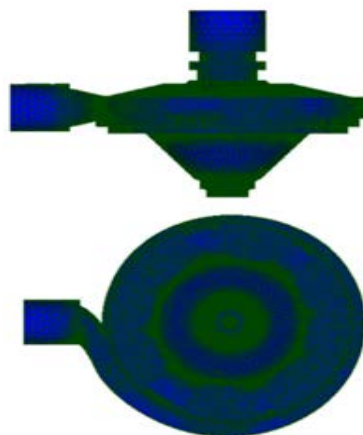


Fig. 5. Mesh defined for the CFD model – Left: Inside, right: Outside

Based on the mesh independence study, shown in Figure 6, it was found that at approximately 400,000 elements the result stabilizes, therefore, 376,431 elements were used for the CFD model.

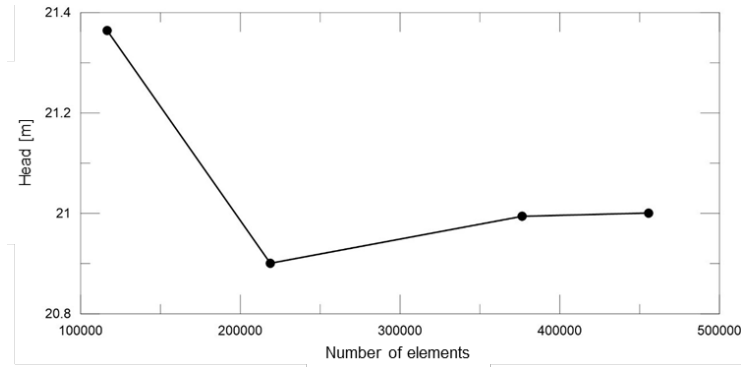


Fig 6. Ratio between the number of elements defined for the mesh and the head delivered by the model

### 2.4.1 Boundary conditions

Velocity at pipe inlet: 2.4 m/s. Pump inlet pressure, set at 101,325 Pa, so that it is compatible with the multiphase model selected in ANSYS.

### 2.4.2 Governance Equations

A volume of fluid (VOF) model was used to obtain the governance equations of the system. These equations were solved using equilibrium equations of momentum and vapor volume fraction for each phase (liquid and vapor).

$$\frac{\partial}{\partial t}(\rho \vec{v}) + \nabla \cdot (\rho \vec{v}) = -\nabla p + \nabla [\mu(\nabla \vec{v} + \nabla \vec{v}^T)] + \rho \vec{g} + \vec{F} \quad (1)$$

$$\frac{\partial \alpha_q}{\partial t} + \vec{v} \cdot \nabla \alpha_q = \frac{S \alpha_q}{\rho_q} = 0 \quad (2)$$

$$\sum_{q=1}^n \alpha_q = 1 \quad (3)$$

### 2.4.3 CFD Simulation

Pressure and vapor volume fraction were examined using CFD techniques. The numerical method was based on the finite volume method (VFM) and the RANS equations using a standard k-epsilon turbulence model. This model was used because it requires a lower computational cost and is robust for a wide range of turbulent flows [23]. Also, for the simulation, the cavitation model of Schnerr and Sauer [24] was considered.

$$\dot{m} = -\frac{\rho_v \rho_l}{\rho_m} (1 - \alpha_v) \cdot \frac{3\alpha_v}{\left[ \frac{3\alpha_v}{(1 - \alpha_v) \left( n_0 \cdot \frac{4}{3} \pi \right)} \right]^{\frac{1}{3}}} \sqrt{\frac{2 p_{sat} - p}{3 \rho_l}} \quad (4)$$

### 2.5 Validation

The model was validated through comparison of the head and NPSH curves given by the manufacturer and the ones generated by the simulation, as shown in Figures 7 and 8.

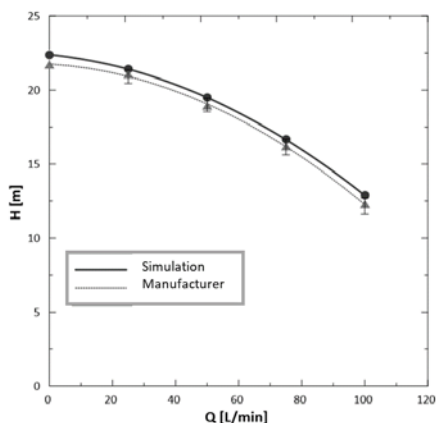


Fig. 7. Head curves given by manufacturer and generated by simulation

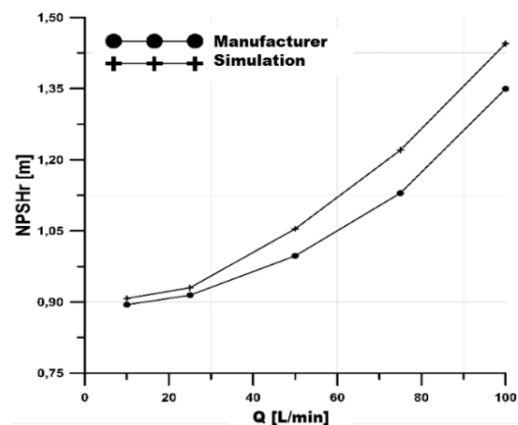


Fig. 8. NPSHr curves from manufacturer and generated by simulation

The relative error for the highest scattered values between the graphs is:

- Head

$$\%E = \frac{|22.5 - 22|}{22} * 100\% = 2.27\%$$

- NPSH

$$\%E = \frac{|1.42 - 1.36|}{1.36} * 100\% = 4.41\%$$

Since the error found in both cases is less than 5%, it is concluded that the model and its simulation are valid.

## 2.6 Configuration

Table 1 shows the temperatures, in °C, considered in this investigation, as well as the rotation speed for this set of simulations. Table 2 contains the rotational speeds (constant temperature), in RPM, and Table 3 shows the diameters for the suction pipe, in inches, and the type of reducer (constant speed and temperature).

Table 1. Water temperature

Item	Temperature [°C]	Rotational speed [RPM]
1	17	3.500
2	22	3.500
3	27	3.500
4	32	3.500
5	37	3.500

Table 2. Pump rotation speed.

Item	Rotational speed [RPM]	Temperature [°C]
1	3.000	22
2	3.250	22
3	3.500	22
4	3.750	22
5	4.000	22

Table 3. Suction pipe diameter and reducer type.

Item	Suction pipe diameter [in.]	Temperature [°C]	Rotational speed [RPM]
1	1 ¼	22	3.500
2	1 ½	22	3.500
3	1 ½	22	3.500
4	2	22	3.500

## 3 RESULTS AND DISCUSSIO

This section shows the results of the simulations. The contours of pressure and volume fraction of vapor through the impeller were plotted. To set up the comparisons between the different arrangements, 4 parameters were taken into consideration. These parameters were the minimum pressure in the impeller, the vapor pressure, the cavitation number, and the NPSHr.

### 3.1 Temperature variation

By performing the variation of the first configuration at different temperatures (stated in Table 1), the pressure contours and the volume fraction of vapor present in the fluid as it passes through the impeller are obtained in Figure 9. Pressures between 5,561 Pa and 318,200 Pa were obtained. In addition, the minimum pressures, in each case,

are located right in the impeller eye. On the other hand, vapor volume fractions between 0 and 0.7653 were obtained, the maximum value being in the impeller eye.

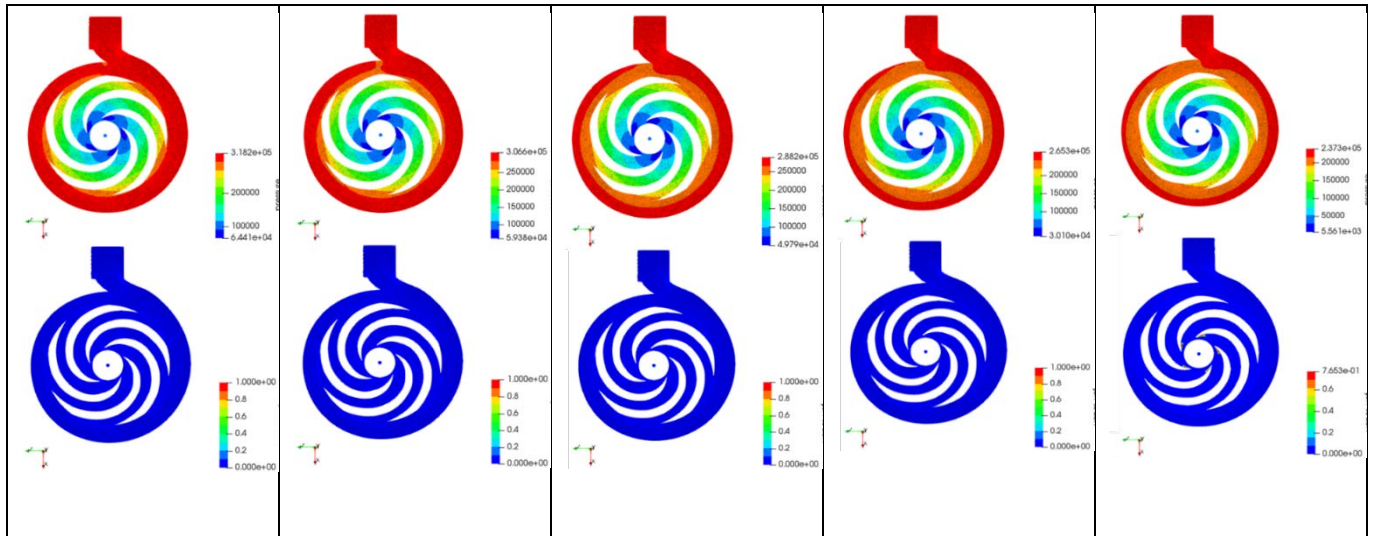


Fig. 9. Pressure contours and vapor volume fraction through the impeller – left to right: 17°C, 22°C, 27°C, 32°C, 37°C

Figure 10 compares the minimum pressure across the impeller with the vapor pressure at different temperatures. A decreasing parabolic relationship was obtained in the minimum pressure with respect to the temperature change. At 37°C the minimum pressure (5,561 Pa) falls below the saturation pressure of the fluid (6,279.5 Pa), at all other temperatures the minimum pressure remains above the vapor pressure. This graph is plotted with the intention of verifying safe operating zones, which, in this case, occurs when the temperature is below 37°C. Figure 11 shows the behavior of the vapor volume fraction at different temperatures. It was found that there is only one vapor volume fraction value different from 0 at 37°C and it corresponds to the value of 0.7653. This indicates that at this temperature there are vapor pockets in the fluid, meaning that the pump is cavitating.

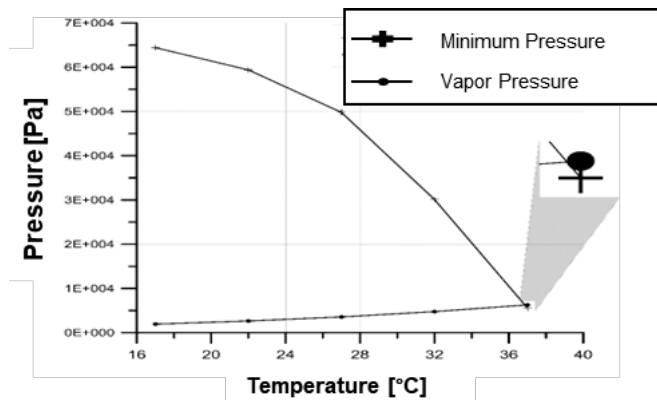


Fig. 10. Temperature and pressure

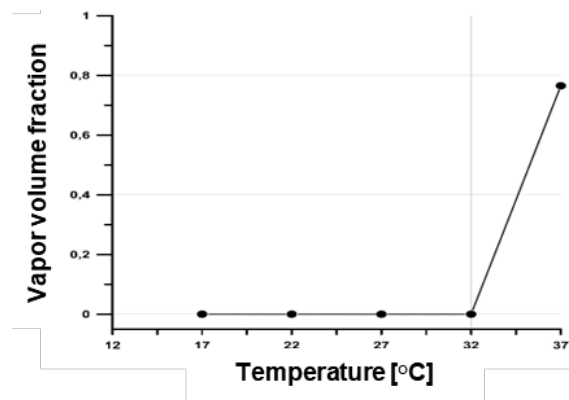


Fig. 11. Vapor volume fraction at different temperatures

The cavitation number is a dimensionless quantity that measures the difference between the local fluid pressure and the vapor pressure of the fluid compared to the kinetic energy (Eq. 5). This dimensionless number gives a measure of the potential for cavitation to take place, so a cavitation number close to 0 indicates that the potential for cavitation to occur is high. [25]. Figure 12 shows the cavitation number for different temperatures. For 37°C this number becomes negative (-0.029), because the local pressure is lower than the vapor pressure, indicating that cavitation is already occurring. In addition, it was identified that exceeding 32°C should be avoided, because, from this temperature, the value of the cavitation number is less than 1, increasing the potential for cavitation to occur.

$$Ca = \frac{p - p_v}{\frac{1}{2} \rho v^2} \quad (5)$$

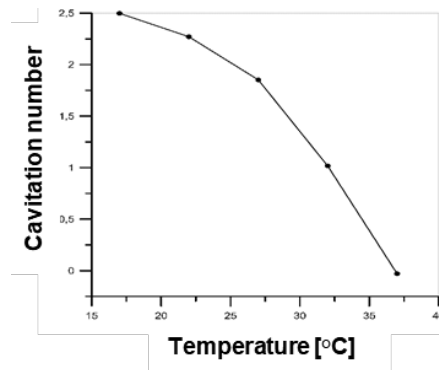


Fig. 12. Cavitation number and temperature

Figures 10-12 indicate that the increase in temperature increases the possibility of cavitation occurrence, this is explained by the fact that the increase in fluid temperature increases the vapor saturation pressure, and, conversely, decreases the minimum pressure in the pump. The study by Abu-Rahmeh et al. showed experimentally that the increase in temperature induces a higher pressure drop which causes a higher chance of cavitation occurrence [26], which corresponds to what was found by CFD in this research.

### 3.2 Rotation speed variation

Figure 13 show the pressure contours and the vapor volume fraction as a function of the rotational speed of the impeller. Figure 14 shows the relation between the minimum pressure and the vapor pressure with respect to the rotational speed in Table 2.

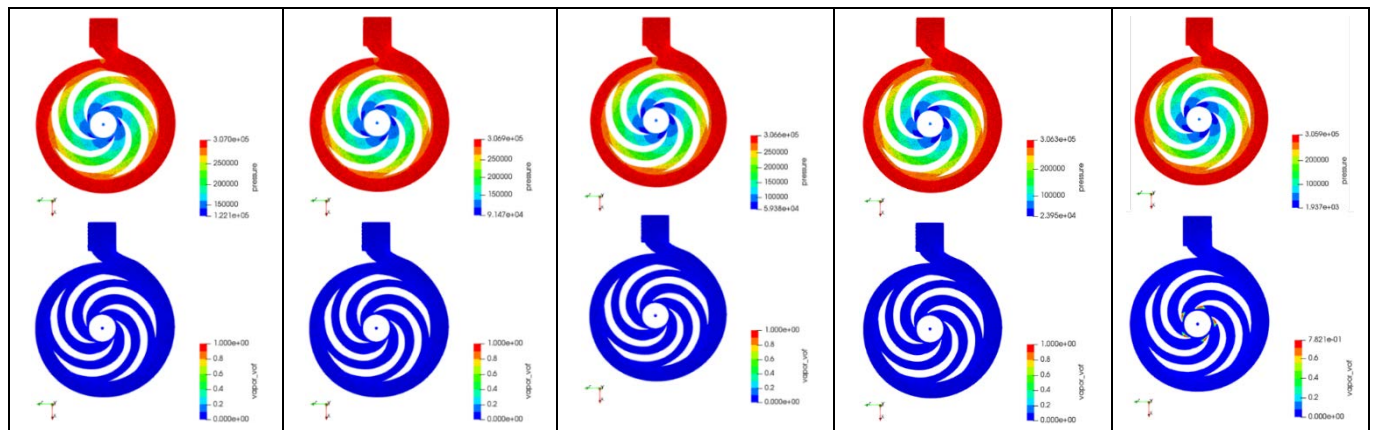


Fig. 13. Vapor Volume Fraction and Pressure Contours – Left to right: 3,000 rpm, 3,250 rpm, 3,500 rpm, 3,750 rpm, right: 4,000 rpm

Figure 14 shows the relationship between minimum pressure and vapor pressure versus rotational speed. The minimum pressure decreases almost linearly with the rotation speed. This behavior is the result of increasing the tangential velocity of the fluid, which generates a decrease in its pressure. The vapor pressure remains constant because the temperature for all rotation speeds is the same (22°C). From Figure 14, it is identified that at 4,000 RPM the minimum local pressure (1,937 Pa) is lower than the vapor pressure (2,643.4 Pa). In turn, Figure 15 shows that at this speed of rotation there is a vapor volume fraction equal to 0.7821. This indicates that the pump is cavitating at that speed.

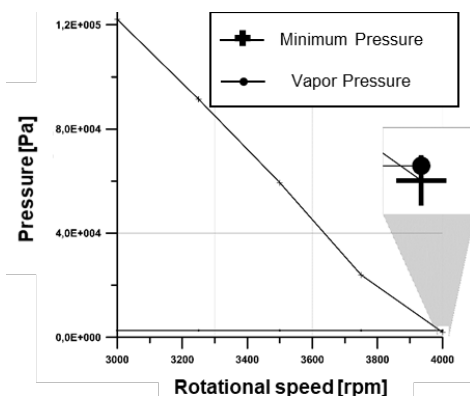


Fig. 14. Variation of the minimum pressure in the center of the impeller with respect to the speed of rotation

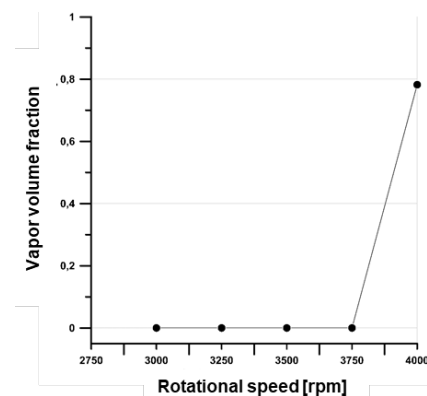


Fig. 15. Variation of the vapor volume fraction with respect to the rate of rotation

Moreover, the NPSHr is another important parameter for predicting the occurrence of cavitation, so the relationship between NPSHr and flow rate is analyzed. Figure 16 shows the behavior of NPSHr with respect to the flow rate driven by the pump and the rotational speed. The NPSHr increases as a function of rotational speed, which indicates that the suction conditions must be controlled to prevent cavitation.

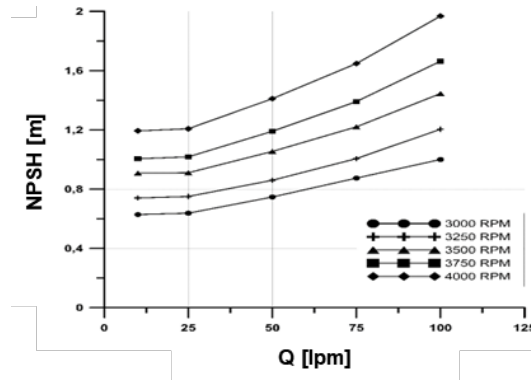


Fig. 16. Variation of NPSHr with respect to flow rate and rotational speed

Hu et al. through their research with CFX found that, under the same pressure conditions at the pump inlet, the increase of the rotational speed brings about the appearance of cavitation phenomenon [27], which corresponds to that shown in Figures 13-16. This is explained by the fact that increasing the rotational speed increases the fluid velocity through the pump, which generates a higher pressure drop, both due to friction and to the transformation of energy in the form of pressure to kinetic energy.

### 3.3 Variation of suction pipe diameter and reducer type

Figure 17 shows the contour map of both the pressure and vapor volume fraction throughout the impeller versus the geometry of the suction pipe and the type of reducer coupling used (Table 3). In the case of eccentric reducers, the flat side was placed at the top. This configuration was chosen because this position reduces the pressure drop in the fitting and prevents the formation of air pockets in the suction. Pressures between 1,952 Pa and 61,340 Pa were obtained.

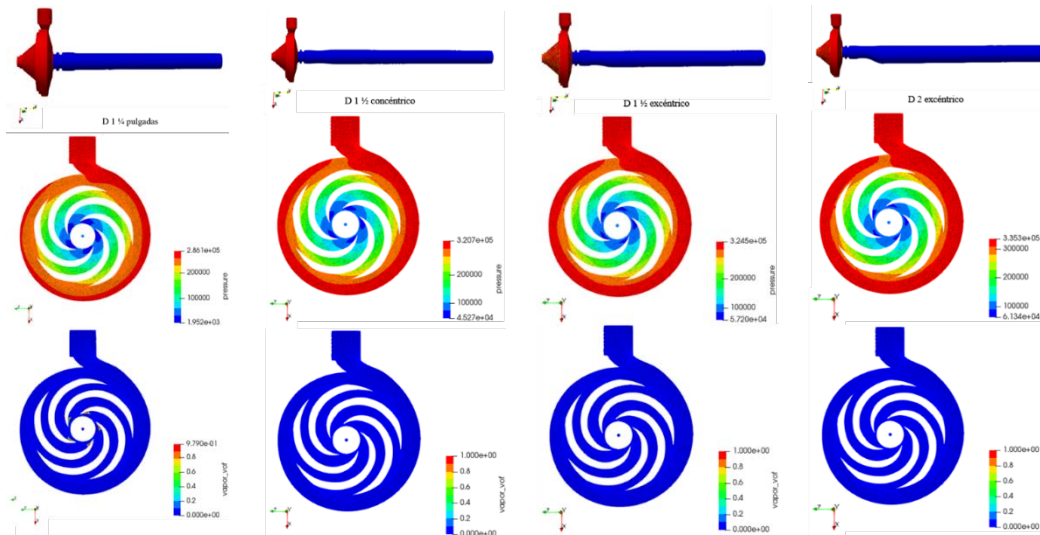


Fig. 17. Pressure contours and steam volume fraction through the impeller – From left to right: 1 1/4" pipe, 1 1/2" pipe with concentric reducer, 1 1/2" pipe with eccentric reducer, 2" pipe with eccentric reducer

Figure 18 shows that the minimum fluid pressure (1,952 Pa) is less than the vapor pressure (2,643.4 Pa) when the pipe has a diameter of 1.25 in. (1 1/4"), generating steam pockets in the impeller eye (Figure 17a).

Figures 20 and 21 show that increasing the diameter prevents pressure drop at the pump inlet. This is because, by continuity, keeping the flow rate constant, the speed of the fluid decreases as the diameter increases. This velocity of the fluid is linked to the friction losses in the pipe, and, consequently, to the pressure drop in the suction.

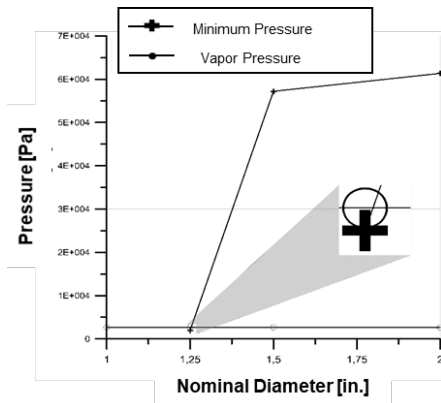


Fig. 20. Variation of the minimum pressure in the pump with respect to the diameter of the suction pipe (red. eccentric).

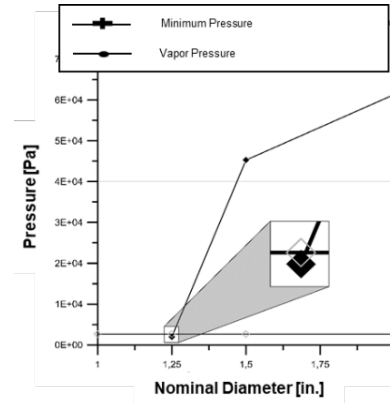


Fig. 21. Variation of the minimum pressure in the pump with respect to the diameter of the suction pipe (red. concentric).

#### 4 CONCLUSIONS

In the present research, a CFD model was developed and validated to study the effect of parameter variation in the operation of a centrifugal pump, generating strategies that allow the safe operation of this device against cavitation. The research demonstrated that the use of CFD tools allows, in a simpler way than physical experimentation, the collection of information and the change in operating conditions without losing accuracy in the results, as shown by the validation of the model, in which errors of less than 5% were obtained. The tetrahedral mesh type, the Schnerr and Sauer cavitation model and the standard  $k - \epsilon$  turbulence model allow the simulation of water flows in centrifugal pumps with low computational costs and high accuracy. It is recommended to control the operating temperature, since an increase of only a few degrees can lead to equipment cavitation. As shown in the study, from 32°C onwards, the effect of temperature on the cavitation occurrence potential is accentuated, evidenced in higher pressure drops, in the increase of the fluid vapor pressure and in the decrease of the cavitation number.

It is recommended to control the rotational speed, because, as shown in the research, the increase in RPM generates an increase in the NPSHr of the pump, thus increasing the potential for cavitation to occur in the device. The suction pipe should have a larger diameter than the suction diameter of the pump, since the fluid velocity is reduced and, in turn, the friction losses in the suction. This implies a lower pressure drop in the suction, reducing the potential for cavitation in the centrifugal pump. The pressure and vapor volume fraction contours plotted allow the identification of the area most susceptible to the occurrence of the cavitation phenomenon in the pump and allow the establishment of safe operating conditions within the established parameters. This validated CFD methodology allows to establish safe operating conditions against cavitation, generating lower costs than a physical test bench and with practicality to make changes in the operating parameters. In addition, it can be replicated to other similar centrifugal pumps.

#### Nomenclature

$\alpha_v$	Vapor Volume Fraction
Ca	Cavitation number
g	Gravity [m/s <sup>2</sup> ]
$\dot{m}$	Mass flow of water [kg/s]
$n_0$	Number of cavitation nuclei per unit volume
NPSHr	Net positive suction head required [m]
$\rho$	Water density [kg/m <sup>3</sup> ]
$\rho_l$	Liquid state density [kg/m <sup>3</sup> ]
$\rho_v$	Density of the gaseous state [kg/m <sup>3</sup> ]
p	Water pressure [kPa]
$p_{sat}$	Water saturation pressure [kPa]
$\mu$	Dynamic viscosity of water [kg/m s]
v	Water velocity [m/s]

## 5 REFERENCES

- [1] L. Bachus and A. Custodio, "Know and understand centrifugal pumps: by Larry Bachus and Angel Custodio" World Pumps, vol. 2003, no. 446, p. 4, Nov. 2003, doi: 10.1016/S0262-1762(03)01102-7.
- [2] R. Johnson, Handbook of Fluid Dynamics, 2nd ed. 2016.
- [3] J. K. Myung, B. J. Hyun, and J. C. Wui, "A Study on Prediction of Cavitation for Centrifugal Pump," World Academy of Science, Engineering and Technology. International Journal of Mechanical and Mechatronics Engineering., vol. 6, 2012.
- [4] B. K. Sreedhar, S. K. Albert, and A. B. Pandit, "Cavitation damage: Theory and measurements – A review," Wear, vol. 372–373, pp. 177–196, Feb. 2017, doi: 10.1016/J.WEAR.2016.12.009.
- [5] F. Zhang, S. Yuan, Q. Fu, J. Pei, M. Bohle, and X. Jiang, "Cavitation-induced unsteady flow characteristics in the first stage of a centrifugal charging pump," Journal of Fluids Engineering, Transactions of the ASME, vol. 139, no. 1, Jan. 2017, doi: 10.1115/1.4034362/373048.
- [6] B. K. Sreedhar, S. K. Albert, and A. B. Pandit, "Cavitation damage: Theory and measurements – A review," Wear, vol. 372–373, pp. 177–196, Feb. 2017, doi: 10.1016/J.WEAR.2016.12.009.
- [7] N. Zhang, M. Yang, B. Gao, and Z. Li, "Vibration characteristics induced by cavitation in a centrifugal pump with slope volute," Shock and Vibration, vol. 2015, Jan. 2015, doi: 10.1155/2015/294980.
- [8] B. Gao, P. Guo, N. Zhang, Z. Li, and M. Yang, "Experimental Investigation on Cavitating Flow Induced Vibration Characteristics of a Low Specific Speed Centrifugal Pump," Shock and Vibration, vol. 2017, 2017, doi: 10.1155/2017/6568930.
- [9] R. Azizi, B. Attaran, A. Hajnayeb, A. Ghanbarzadeh, and M. Changizian, "Improving accuracy of cavitation severity detection in centrifugal pumps using a hybrid feature selection technique," Measurement, vol. 108, pp. 9–17, Oct. 2017, doi: 10.1016/J.MEASUREMENT.2017.05.020.
- [10] J. Lu, S. Yuan, P. Siva, J. Yuan, X. Ren, and B. Zhou, "The characteristics investigation under the unsteady cavitation condition in a centrifugal pump," Journal of Mechanical Science and Technology, vol. 31, no. 3, pp. 1213–1222, Mar. 2017, doi: 10.1007/S12206-017-0220-3.
- [11] D. Alberto et al., "Computational Analysis of Different Turbulence Models in a Vane," | Indonesian Journal of Science & Technology, vol. 6, no. 1, p. 160, 2021, doi: 10.17509/ijost.v6i1.xxxx.
- [12] L. Hanimann, L. Mangani, E. Casartelli, and M. Widmer, "Cavitation modeling for steady-state CFD simulations," IOP Conference Series: Earth and Environmental Science, 2016. doi: 10.1088/1755-1315/49/9/092005.
- [13] R. N. Pinto, A. Afzal, L. V. D'Souza, Z. Ansari, and A. D. Mohammed Samee, "Computational Fluid Dynamics in Turbomachinery: A Review of State of the Art," Archives of Computational Methods in Engineering, vol. 24, no. 3, pp. 467–479, Jul. 2017, doi: 10.1007/S11831-016-9175-2.
- [14] Z. Qin and H. Alehossein, "Heat transfer during cavitation bubble collapse," Applied Thermal Engineering, vol. 105, pp. 1067–1075, Jul. 2016, doi: 10.1016/J.APPLTHERMALENG.2016.01.049.
- [15] S. Fujikawa and T. Akamatsu, "Effects of the non-equilibrium condensation of vapour on the pressure wave produced by the collapse of a bubble in a liquid," Journal of Fluid Mechanics, vol. 97, no. 3, pp. 481–512, 1980, doi: 10.1017/S0022112080002662.
- [16] J. Lu, S. Yuan, P. Siva, J. Yuan, X. Ren, and B. Zhou, "The characteristics investigation under the unsteady cavitation condition in a centrifugal pump," Journal of Mechanical Science and Technology 2017 31:3, vol. 31, no. 3, pp. 1213–1222, Mar. 2017, doi: 10.1007/S12206-017-0220-3.
- [17] R. B. Medvitz, R. F. Kunz, D. A. Boger, J. W. Lindau, A. M. Yocum, and L. L. Pauley, "Performance analysis of cavitating flow in centrifugal pumps using multiphase CFD," Journal of Fluids Engineering, Transactions of the ASME, vol. 124, no. 2, pp. 377–383, 2002, doi: 10.1115/1.1457453.
- [18] B. K. Sreedhar, S. K. Albert, and A. B. Pandit, "Cavitation damage: Theory and measurements – A review," Wear, vol. 372–373, pp. 177–196, Feb. 2017, doi: 10.1016/J.WEAR.2016.12.009.
- [19] S. Hattori and M. Kishimoto, "Prediction of cavitation erosion on stainless steel components in centrifugal pumps," Wear, vol. 265, no. 11–12, pp. 1870–1874, Nov. 2008, doi: 10.1016/J.WEAR.2008.04.045.
- [20] L. Alfayez, D. Mba, and G. Dyson, "The application of acoustic emission for detecting incipient cavitation and the best efficiency point of a 60-kW centrifugal pump: Case study," NDT and E International, vol. 38, no. 5, pp. 354–358, Jul. 2005, doi: 10.1016/J.NDTEINT.2004.10.002.
- [21] S. F. Chini, H. Rahimzadeh, and M. Bahrami, "Cavitation detection of a centrifugal pump using noise spectrum," Proceedings of the ASME International Design Engineering Technical Conferences and Computers and Information in Engineering Conference - DETC2005, vol. 1 A, pp. 13–19, 2005, doi: 10.1115/DETC2005-84363.
- [22] Barnes, "BOMBAS CARACOL DE 1 5-1/ DE 1 10-1." [Online]. Available: www.barnes.com.co
- [23] B. Mohammadi and Olivier. Pironneau, Analysis of the K-Epsilon: turbulence model. Chichester West Sussex [etc.]: John Wiley & Sons, 1994.

- [24] A. Niedźwiedzka, "Homogeneous cavitation modeling – Analysis of basics of mathematical formulation of source terms," *MODELOWANIE INŻYNIERSKIE*, vol. 34, no. 65, pp. 75–82, 2017.
- [25] H. Soyama, "Luminescence intensity of vortex cavitation in a Venturi tube changing with cavitation number," *Ultrasonics Sonochemistry*, vol. 71, p. 105389, Mar. 2021, doi: 10.1016/J.ULTSONCH.2020.105389.
- [26] T. Abu-Rahmeh, O. Badran, A. Al-Alawin, N. Nashat y A. Awwad, "The Effect of water Temperature and Flow Rate on Cavitation Growth in Conduits", 2018.
- [27] S. Hu, W. Song, Q. Xu y J. Shi, "The effect of Rotation Speed on Cavitation of Small Flow Micro - High Speed Centrifugal Pump", en 2017 2nd Int. Conf. Mater. Science, Machinery Energy Eng. (MSMEE 2017), Dalian, China, 13–14 de mayo de 2017. Paris, France: Atlantis Press, 2017. Accedido el 20 de junio de 2023. [Online]. Available: <https://doi.org/10.2991/msmee-17.2017.183>

*Paper submitted: 28.11.2022.*

*Paper accepted: 07.07.2023.*

*This is an open access article distributed under the CC BY 4.0 terms and conditions*